materials

MDPI

Communication

Low-Temperature Hydrothermal Synthesis of Rare-Earth-Doped $Sc_2Mo_3O_{12}$ Crystals for Thermally Enhanced Upconversion Luminescence and Optical Temperature Sensing

Yi Zuo [1], Yanlong Cao [1], Yonghong Yang [1], Juan Cai [1], Han Zhang [2] and Junwei Hou [2,*]

[1] Xinjiang Oilfield Company, Karamay 834000, China
[2] State Key Laboratory of Heavy Oil Processing, China University of Petroleum—Beijing at Karamay, Karamay 834000, China
* Correspondence: junweihou@cupk.edu.cn

Highlights

- A low-temperature hydrothermal method was developed to synthesize phase-pure orthorhombic $Sc_2Mo_3O_{12}$ crystals.
- Phase-pure $Sc_2Mo_3O_{12}$ enabled efficient multicolor upconversion luminescence (UCL) under 980 nm excitation.
- Thermally enhanced upconversion emission and optical thermometric performance were achieved over the temperature range of 310–670 K, with a maximum relative sensitivity (Sr) of 0.0028 K^{-1}.

Abstract

Thermal quenching severely limits the application of upconversion phosphors in high-temperature environments. Negative thermal expansion (NTE) materials have attracted considerable attention as promising hosts for enhancing high-temperature luminescence, whereas low-temperature synthesis of $Sc_2Mo_3O_{12}$ remains rarely reported. In this work, phase-pure orthorhombic $Sc_2Mo_3O_{12}$ crystals were synthesized via a low-temperature hydrothermal method. The effects of precursor molar ratio, reaction temperature, reaction time, and surfactant on phase formation were systematically investigated. Under the optimized synthesis conditions, efficient multicolor upconversion luminescence (UCL) was achieved under 980 nm excitation by employing Yb^{3+} as the sensitizer and Er^{3+}, Tm^{3+}, or Ho^{3+} as the activator ions. Only phase-pure $Sc_2Mo_3O_{12}$ exhibited efficient UCL. Furthermore, the temperature- dependent luminescence properties were investigated over the range of 310–670 K, where the upconversion emission intensity continuously increased with temperature and a maximum relative sensitivity (Sr) of 0.0028 K^{-1} was obtained at 310 K based on the fluorescence intensity ratio (FIR) technique. These results demonstrate that phase-pure $Sc_2Mo_3O_{12}$ prepared by a low-temperature hydrothermal method exhibits thermally enhanced UCL and promising optical thermometric performance, highlighting its potential as an NTE host for high-temperature optical temperature sensing.

Keywords: negative thermal expansion; one-pot hydrothermal reaction; scandium molybdate; upconversion luminescence

Check for updates

Academic Editor: Shenyang Huang

Received: 25 September 2026
Revised: 23 October 2026
Accepted: 28 October 2026
Published: 31 October 2026

Copyright: © 2026 by the authors. Licensee MDPI, Basel, Switzerland. This article is an open access article distributed under the terms and conditions of the Creative Commons Attribution (CC BY) license.

1. Introduction

Upconverted luminescent materials are fast becoming a key instrument in the fields of bio-detection, optogenetics, advanced information anti-counterfeiting, optical temperature measurement, near-infrared imaging, and disease theranostics [1–6]. However, the non-radiative relaxation is a leading cause of the thermal quenching (TQ) problem severely limits its practical application and makes it difficult to carry out industrialized production [7–10].

Numerous studies have demonstrated that the NTE property of host materials can effectively enhance luminescence intensity through lattice contraction and distortion during heating, thereby mitigating thermal quenching at elevated temperatures [11–20]. This strategy has significantly broadened the application potential of upconversion luminescent materials in high-temperature environments [21]. Owing to its stable crystal structure and unique NTE behavior, $Sc_2Mo_3O_{12}$ has been widely employed as a host material for rare-earth luminescent phosphors [22]. However, studies on the low-temperature synthesis of $Sc_2Mo_3O_{12}$ phosphors remain scarce.

In this work, we aim to (i) develop a low-temperature hydrothermal route for phase-pure $Sc_2Mo_3O_{12}$ crystals, (ii) investigate the influence of synthesis conditions on morphology and luminescence behavior, and (iii) evaluate their temperature-dependent UCL and optical thermometric performance. This work provides a feasible strategy for the low-temperature synthesis of NTE host materials and offers new insights into overcoming thermal quenching in high-temperature luminescent applications.

2. Materials and Methods

We used innovative techniques based on the recommendations of previous reports to synthesize $Sc_2Mo_3O_{12}$ materials using a one-step hydrothermal method [23]. $Sc(NO_3)_3{\cdot}6H_2O$ (99.99%), $(NH_4)_6Mo_7O_{24}{\cdot}4H_2O$ (99.99%), $Yb(NO_3)_3{\cdot}5H_2O$ (99.99%), $ErH_{12}N_3O_{15}$ (99.99%) was obtained from damas-beta and without processing. The first step in the experiment was to configure all the materials in a certain concentration of solution using distilled water. Subsequently, the four solutions were added dropwise to 14 mL of deionized water and stirred in a PPL liner for 2 h. A white precipitate immediately formed. Sealed and lined with 50 mL stainless steel autoclave and heated for 2 h, heating temperature at 140 °C. The resulting samples were centrifuged, washed, dried at 85 °C and 800 °C for 2 h in an atmospheric environment using a muffle furnace. The synthesis method is shown in Figure 1.

The Phosphor phase composition and lattice parameters were carried out using an X-ray diffractometer (XRD, Ultima IV, Rigaku Corporation, Akishima, Tokyo, Japan). The morphologies and sizes of phosphors were observed by a scanning electron microscope (SEM, ZEISSSigma300, Oberkochen, Germany). UC spectra were recorded by a fluorescence spectrophotometer (F4700, Hitachi, Ltd., Tokyo, Japan) equipped with a 980 nm laser. The testing temperature was controlled by a thermal stage (THMS600, Linkam Scientific Instruments, Tadworth, UK).

In-situ variable-temperature X-ray diffraction (VT-XRD) measurements were carried out on a Bruker D8 Advance diffractometer with Cu Kα radiation (λ = 1.5406 Å) equipped with an Anton Paar HTK1200N high-temperature heating stage. The whole measurement was conducted under a continuous flowing high-purity nitrogen atmosphere to avoid oxidation, hydrolysis and surface contamination of the sample at high temperatures. Diffraction patterns were recorded from 140 °C to 200 °C with a temperature interval of 20 °C. At each target temperature, the sample was held for 8 min to achieve sufficient thermal equilibrium before data collection.

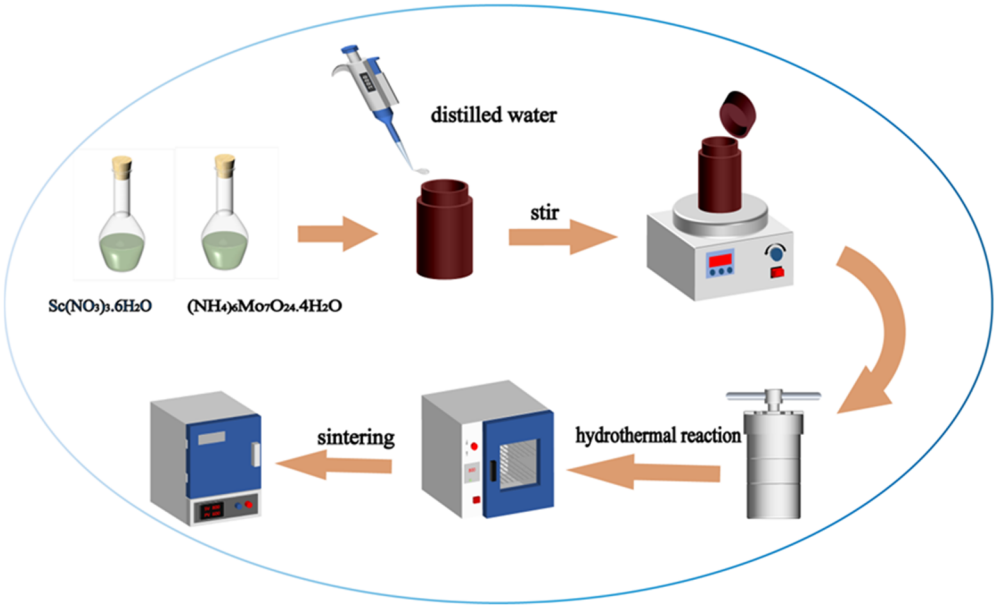


Figure 1. Schematic preparation of $Sc_2Mo_3O_{12}$ using hydrothermal reaction.

3. Results and Discussion

3.1. XRD Composition Analysis

After the completion of the reaction at 140 °C for 2 h according to different molar ratios of Sc:Mo, no crystals of the pure phase were prepared. From Figure 2a, we can see that there is a stray peak at 11.5°, and we guess that it may be the raw material that has not finished the reaction. Then, change the ratio of raw materials, and increase the amount of mo, still at 140 °C reaction 2 h, Figure 2b shows that the heterogeneous peaks are still present. Figure 2c illustrates the XRD patterns of the samples synthesized at Sc:Mo = 2:3 for 2 h in the solution with 140 °C, 160 °C, 180 °C and 200 °C. As shown in Figure 2c, it can be seen that the diffraction intensity is increasing with increasing temperature, but the spurious peaks are still present. Figure 2d illustrates the XRD patterns of the samples synthesized at the same molar ratio for 140 °C in the solution with 2 h, 6 h, 12 h and 24 h. As can be seen from Figure 2d, the diffraction intensity did not change with time and spurious peaks remained.

Phase-pure $Sc_2Mo_3O_{12}$ was finally obtained after painstaking efforts. Crystals with different conditions were prepared according to Sc:Mo = 1:3. Figure 2e shows the XRD pattern of $Sc_2Mo_3O_{12}$ particles at different temperatures for 2 h. The XRD pattern is in excellent agreement with the diffraction peaks of $Sc_2Mo_3O_{12}$ (JCPDF No. 21-1329), demonstrating that $Sc_2Mo_3O_{12}$ has been successfully synthesized via the hydrothermal method. As the temperature increases, the intensity of the diffraction peaks is increasing, and the location of the peaks does not change much. This suggests that increasing the temperature favours the growth of crystals. Figure 2f presents the XRD patterns of $Sc_2Mo_3O_{12}$ synthesized by hydrothermal reaction at 140 °C for different reaction times. It can be seen that the intensity of the diffraction peaks increases with the extension of time, reaching the highest at 12 h, and the intensity of the diffraction peak decreases at 24 h, without much change in the location of the peak.

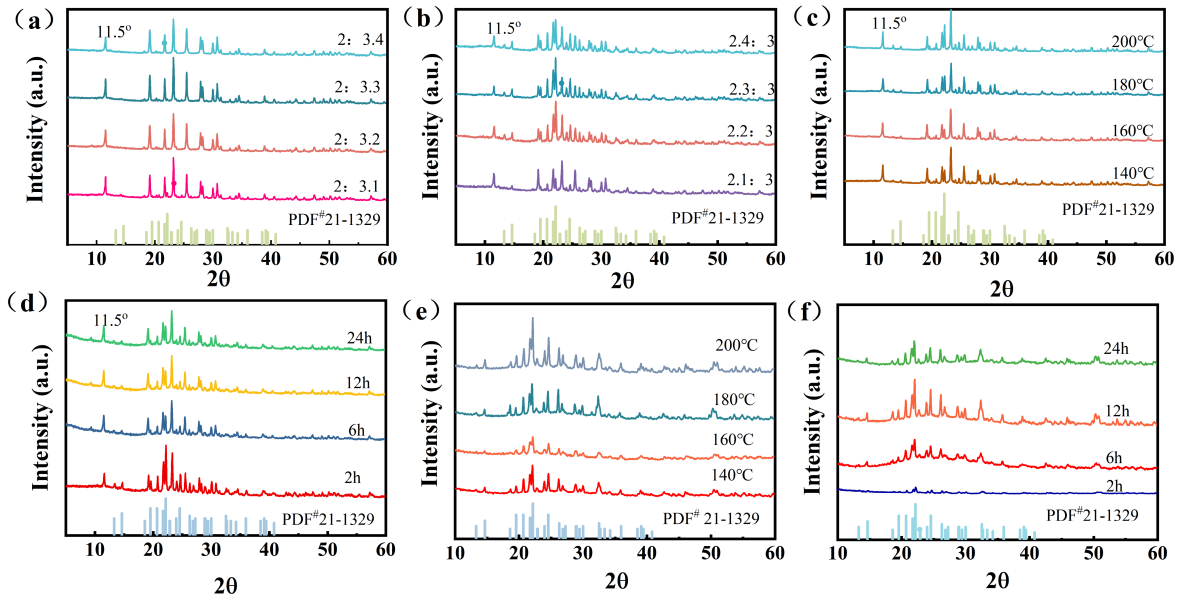


Figure 2. XRD patterns of $Sc_2Mo_3O_{12}$ samples synthesized by hydrothermal reaction under different conditions. (**a**) at 140 °C for 2 h with different mole ratios (**b**) at 140 °C for 2 h with different mole ratios (**c**) at 2 h for various temperatures (**d**) at 140 °C for different times (**e**) at various temperatures for 2 h (**f**) at various time for 140 °C.

3.2. SEM Microscopic Morphology Analysis

Since crystal morphology and surface defects strongly influence luminescence efficiency, surfactant-assisted morphology regulation was further investigated. We used different surfactant assisted hydrothermal methods for surface modification and also performed SEM analysis to determine the microscopic morphology of the $Sc_2Mo_3O_{12}$ crystals. Figure 3 highlights the differences in morphology after modification with EG, CATB and PVP. All reactions were carried out at 220 °C with 0.25 g urea for 24 h. Figure 3a shows the results of the surface morphology after glycol modification, which forms many rod-like and block-like regular structures. Ethylene glycol is miscible with water and can act as a co-solvent and coordinating agent during hydrothermal synthesis, thereby affecting crystal nucleation, growth, and morphology [24]. Figure 3b demonstrates the morphology of the rectangular lamellae formed after modification with CATB. A large number of catb molecules are adsorbed on the crystal surface, lowering the surface energy and directing crystal growth. From the data in Figure 3c, it is apparent that regular pie structures can be synthesized using PVP. PVP, as a water-soluble polymer compound, modifies the surface of nanoparticles to form a stable dispersion system, preventing aggregation and precipitation of nanoparticles [25]. Figure 3d,e can support this idea. We have successfully synthesized morphologically regular nano single crystals as can be seen in Figure 3f. Appendix A shows the XRD results of $Sc_2Mo_3O_{12}$ materials modified with PVP, EG and CTAB, respectively. It can be observed that the diffraction peak intensity decreases slightly, while the peak positions remain almost unchanged. This confirms that the surfactants only regulate the crystal morphology without altering the crystal phase.

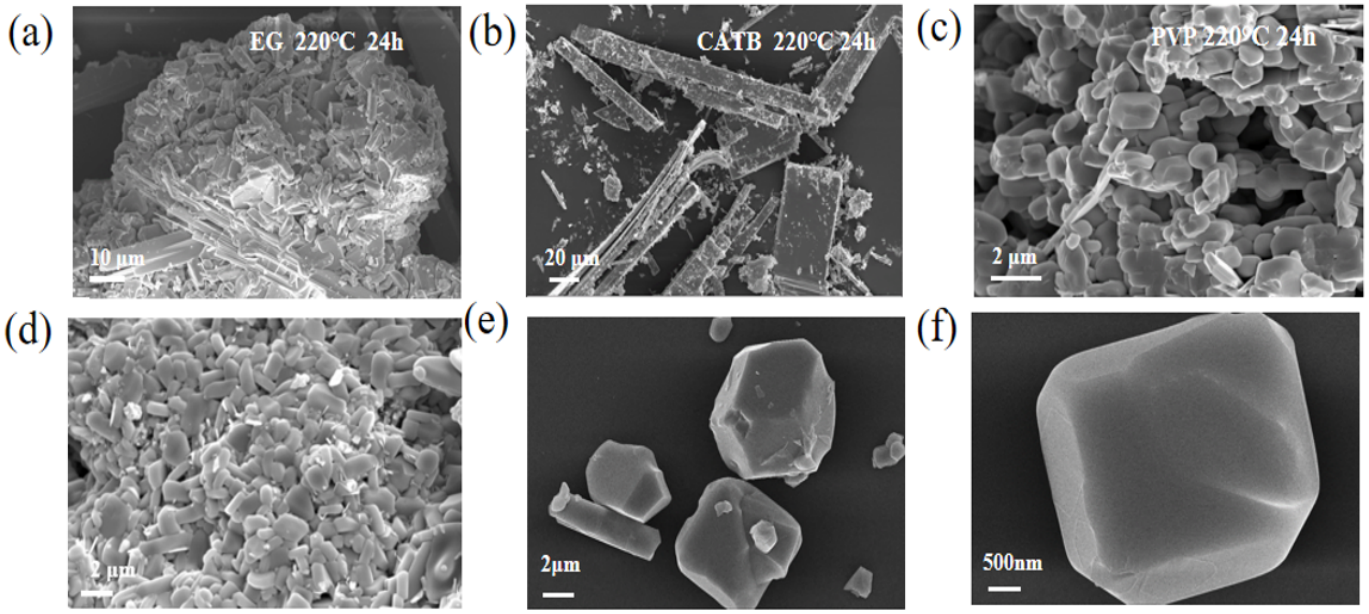


Figure 3. SEM images of $Sc_2Mo_3O_{12}$ samples synthesized by hydrothermal reaction under different surfactants (**a**) at 220 °C for 24 h with 0.25 g ethylene glycol (**b**) with 0.25 g CATB (**c**) with 0.25 g PVP (**d**–**f**) microscopic morphology using PVP modification.

3.3. Up-Conversion and Down-Conversion Spectra

Yb^{3+} ions were introduced as sensitizers due to their efficient 980 nm absorption, while Er^{3+}, Tm^{3+} and Ho^{3+} ions served as activators for generating multicolor emission.Figure 4a shows the UC emission spectra of the $Sc_2Mo_3O_{12}$:Yb/Er (18%Yb, 1%Er) crystals under 980 nm excitation at room temperature. The green emission peaks at 524 and 559 nm are attributed to $^2H_{11/2} \rightarrow {}^4I_{15/2}$ and $^4S_{3/2} \rightarrow {}^4I_{15/2}$ transitions of Er^{3+} ions. Figure 4b [26] showsthe UC spectra of the Yb/Ho-codoped $Sc_2Mo_3O_{12}$ crystals under 980 nm excitation. We can observe intense red emission at 554 nm and 664 nm which are assigned to $^5F_4$, $^5S_2 \rightarrow {}^5I_8$ and $^5F_5 \rightarrow {}^5I_8$ transitions, respectively, of Ho^{3+} ion. Figure 4c [27] shows the emission of blue light is mainly due to the $^3H_6 \rightarrow {}^1G_4$ of Tm^{3+} ion.

$Sc_2Mo_3O_{12}$ crystals also have excellent down-conversion luminescence properties. We measured the down-conversion emission spectra of samples doped with Yb/Er, Yb/Tm, and Yb/Ho with different doping concentrations under 980 nm laser excitation at room temperature, as shown in Figure 4d–f. Figure 4d demonstrates that down-conversion luminescence spectra of $Sc_2Mo_3O_{12}$: Yb/Er (Yb: 5%, 10%, 15%, Er: 2%; Er:0.5%, 1%, 2%, 4%, Yb: 18%) with different doping concentrations. The highest fluorescence intensity was detected when the sensitizer was doped at a concentration of 5%. The characteristic emission peaks at 1525 nm NIR-IIb were attributed to $^4I_{13/2} \rightarrow {}^4I_{15/2}$ levels of the Er^{3+} ion, respectively. Yb^{3+} ions can act as energy traps to capture more energy effectively increasing luminescence in the near-infrared second region [28]. Then, the spectra demonstrated by Figure 4e,f are relatively simple compared to the up conversion spectra. Only infrared emission is observed in 1000–1150 nm, and the emission peak can be attributed to $^2F_{5/2} \rightarrow {}^2F_{7/2}$ levels of Yb^{3+} ion. $Sc_2Mo_3O_{12}$: Yb/Tm (Yb: 5%, 10%, 15%, Tm: 2%; Tm: 0.5%, 1%, 2%, 4%, Yb: 18%) $Sc_2Mo_3O_{12}$: Yb/Ho (Yb: 5%, 10%, 15%, Ho: 2%; Ho: 0.5%, 1%, 2%, 4%, Yb: 18%).

An important aspect was observed in these experiments, in which the fluorescence intensity could only be detected with pure-phase and well-ordered scandium crystals as the host material. Good morphology and stable nuclei contribute to efficient up conversion fluorescence from nanocrystals $Sc_2Mo_3O_{12}$:x%Yb/Ln (Er, Tm, Ho).

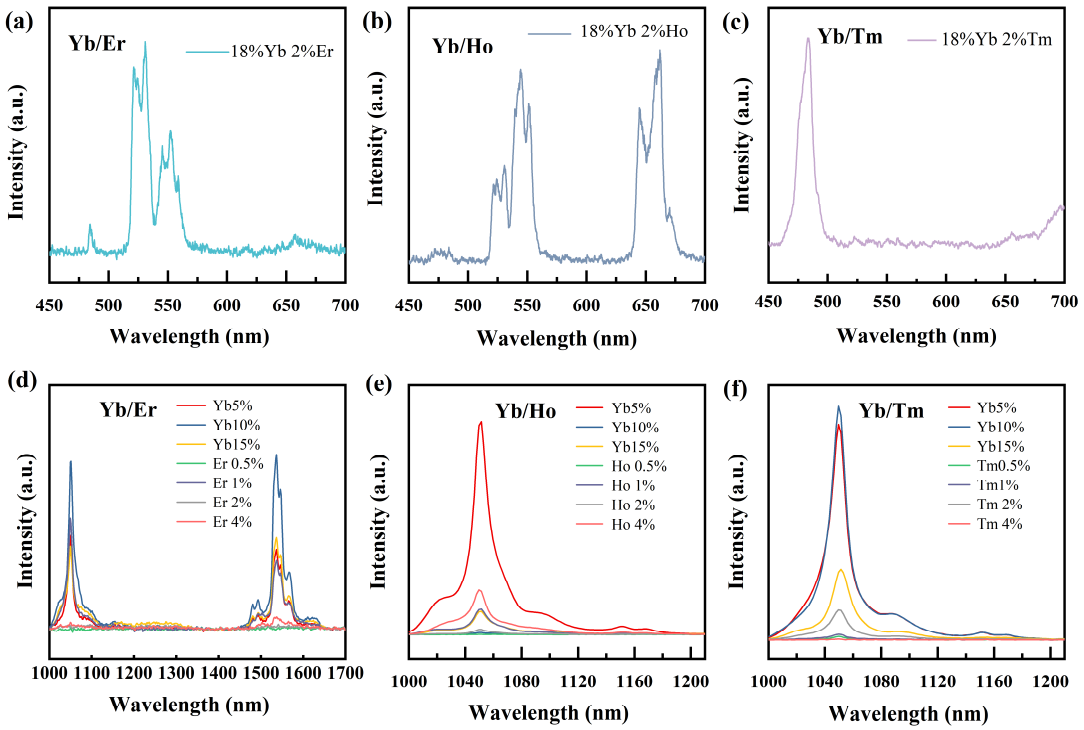


Figure 4. Upconversion emission spectra of $Sc_2Mo_3O_{12}$ doped with (**a**) Yb/Er, (**b**) Yb/Tm, (**c**) Yb/Ho. Downconversion emission spectra of $Sc_2Mo_3O_{12}$ doped with different molar ratios of (**d**) Yb/Er (**e**) Yb/Tm, (**f**) Yb/Ho.

3.4. UCL Fluorescent Temperature Sensing

Conventional materials expand upon heating, which reduces the energy transfer efficiency and weakens luminescence. In contrast, negative thermal expansion materials contract with increasing temperature and exhibit enhanced luminescence, laying a foundation for their application in optical thermometry. Figure 5 presents the high-resolution XRD patterns of $Sc_2Mo_3O_{12}$ measured from 140 °C to 200 °C. The (112) diffraction peak (the strongest diffraction peak of this material) shifts rightward by 0.1° from 23.22° to 23.32°. Calculations based on Bragg's law demonstrate that the interplanar spacing decreases by 0.00162 nm, confirming the reduction of interplanar spacing as temperature rises. Figure 6a shows the evolution of UCL spectra of $Sc_2Mo_3O_{12}$:Yb/Er (18% Yb, 2% Er) under 980 nm excitation when the temperature increases from 310 K to 670 K. It can be observed that the luminescence intensity rises with increasing temperature without luminescence quenching.

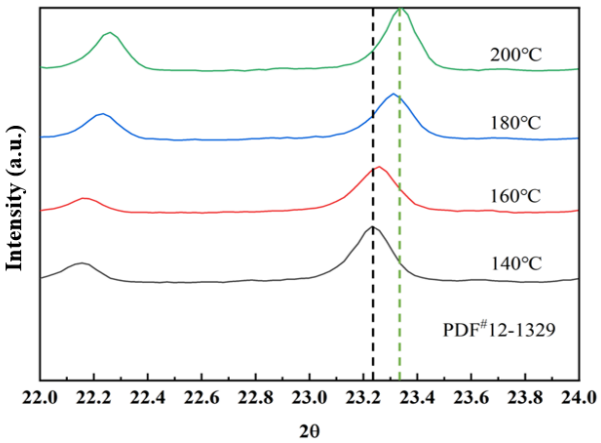


Figure 5. The high-resolution XRD patterns of the sample at different temperatures.

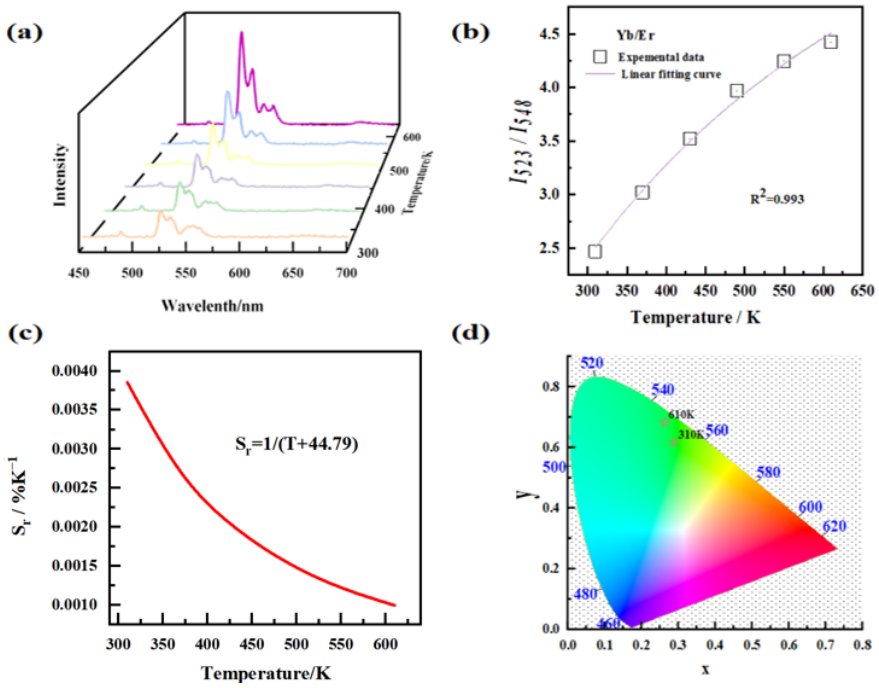


Figure 6. (**a**) UC emission spectra of $Sc_2Mo_3O_{12}$: Yb/Er crystals at various temperatures The FIR (I_{523}/I_{548}) (**b**) as a function of temperature and (**c**) relative sensitivity (**d**) Commission International de I'Eclairage (CIE) chromaticity coordinates of optical emission from the $Sc_2Mo_3O_{12}$:Yb/Er microcrystals with a different temperature.

Figure 6a shows the UCL spectra of $Sc_2Mo_3O_{12}$:Yb/Er(18%Yb, 2%Er) in 310–670K, It can be seen that the fluorescence intensity increases with increasing temperature, and does not show decay. The Yb^{3+} and Er^{3+} thermal enhancement can be further used to achieve fluorescence intensity ratio thermometry. The relative intensity ratio fir of the radiative jumps of the two thermally coupled energy levels can be expressed as Equation (1).

$$\mathrm{FIR} = C\exp\left(\frac{-\Delta E}{K_B T}\right) \quad (1)$$

where C is a constant, ΔE is energy gap between I_{523} and I_{524}, K_B is Boltzmann constant, and the T is absolute temperature. The temperature-dependent FIR (I_{523}/I_{558}) was shown in Figure 6b. In accordance with the FIR technique, FIR can be fitted well with a linear function which exhibits high fitting degrees ($R^2 \geq 0.99$).

Besides, the sensitivity of sensors plays a vital role in temperature measurement. According to the definitions, the relative sensitivity Sr can be expressed by ref. [29]. As an important flatness for evaluating the performance of temperature sensors, The formula for Sr as Equation (1).

$$Sr = \left|\frac{1}{FIR}\frac{dFIR}{dT}\right| = \frac{\Delta E}{KT^2} \quad (2)$$

According to Formula (2), the temperature measurement method based on the I_{524}/I_{559} fluorescence intensity ratio at 310 K in the 310–670 K temperature range yields the maximum Sr. The Sr is maximum of 0.0028 K^{-1} (310 K). Presentation based on Figure 6d CIE1931, it is very straightforward to see that from 310 K to 670 K Er^{3+} are mainly concentrated in green light. The maximum sensitivity and the temperature measurement range of Yb^{3+}/Er^{3+} in various hosts are shown in Table 1.

Table 1. Comparative analysis of temperature sensing properties of lanthanide-doped optical materials.

Materials	λ_{ex} (nm)	λ_{em} (nm)	Temperature Range(K)	MaxS$_r$ (%K^{-1})	Reference
$NaYbF_4$:Er@$NaYbF_4$:Tm	980	520,540	300–405	1.2	[30]
$CaTiO_3$:Nd/Yb/Er	808	524,662	303–573	0.17	[31]
Y_2O_2S:Er/Yb/Tm	980	553,797	303–573	0.080	[32]
$LuYO_3$:Er/Yb	980	523,553	298–848	0.0167	[33]
Gd2O3:Yb/Er	980	522,562	252–413	0.022	[34]
K_3LuF_6:Er,Yb	980	546,662	79–579	1.31	[35]
$Sc_2Mo_3O_{12}$:Yb/Er	980	523,548	310–670	0.003	This work

4. Conclusions

In summary, a low-temperature hydrothermal method was successfully developed for the synthesis of phase-pure orthorhombic $Sc_2Mo_3O_{12}$ crystals. The effects of precursor molar ratio, reaction temperature, reaction time, and surfactant on the phase formation and crystal morphology were systematically investigated, leading to the successful preparation of phase-pure $Sc_2Mo_3O_{12}$ crystals. Using phase-pure $Sc_2Mo_3O_{12}$ as the host, efficient multicolor UCL was realized under 980 nm excitation by employing Yb^{3+} as the sensitizer and Er^{3+}, Tm^{3+}, or Ho^{3+} as the activator ions. More importantly, the phase-pure $Sc_2Mo_3O_{12}$ host exhibited thermally enhanced UCL over the temperature range of 310–670 K without obvious thermal quenching. Furthermore, optical thermometric performance based on the FIR technique was demonstrated, yielding a maximum Sr of 0.0028 K^{-1} at 310 K. These results demonstrate that low-temperature synthesized $Sc_2Mo_3O_{12}$ is a promising NTE host for thermally enhanced UCL and high-temperature optical thermometry, providing a feasible strategy for the low-temperature synthesis of NTE upconversion host materials and offering new insights into overcoming thermal quenching in high-temperature luminescent applications.

Author Contributions: Conceptualization, Y.Z. and Y.C.; methodology, Y.Y.; software, J.C.; validation, H.Z.; formal analysis, Y.C.; investigation, Y.Y.; resources, J.C.; data curation, H.Z.; writing—original draft preparation, Y.Z.; writing—review and editing, J.H.; visualization, Y.C.; supervision, J.H.; project administration, J.H.; funding acquisition, J.H. All authors have read and agreed to the published version of the manuscript.

Funding: This research received financial backing from multiple sources: Tianshan Talent Fund of Xinjiang Province (2023TSYCJC0065), National Natural Science Foundation of China (52360003).

Data Availability Statement: The authors confirm that the data supporting the findings of this study are available within the article.

Conflicts of Interest: Authors Yi Zuo, Yanlong Cao, Yonghong Yang, and Juan Cai were employed by the company. The remaining authors declare that the research was conducted in the absence of any commercial or financial relationships that could be construed as a potential conflict of interest.

Appendix A

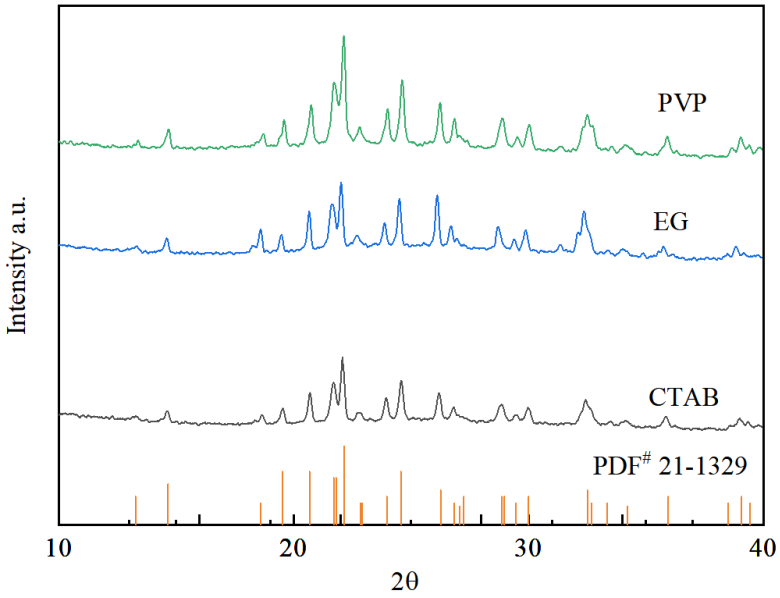


Figure A1. The XRD patterns of $Sc_2Mo_3O_{12}$ materials modified with PVP, EG and CTAB.

References

1. Mun, K.R.; Kyhm, J.; Lee, J.Y.; Shin, S.; Zhu, Y.; Kang, G.; Kim, D.; Deng, R.; Jang, H.S. Elemental-Migration-Assisted Full-Color-Tunable Upconversion Nanoparticles for Video-Rate Three-Dimensional Volumetric Displays. *Nano Lett*. **2023**, *23*, 3014–3022. [CrossRef]
2. Debasu, M.L.; Ananias, D.; Pinho, S.L.C.; Geraldes, C.F.G.C.; Carlos, L.D.; Rocha, J. (Gd,Yb,Tb)PO_4 up-conversion nanocrystals for bimodal luminescence–MR imaging. *Nanoscale* **2012**, *4*, 5154–5162. [CrossRef]
3. Zi, Y.; Yang, Z.; Xu, Z.; Bai, X.; Ullah, A.; Khan, I.; Haider, A.A.; Qiu, J.; Song, Z.; Wang, Y.; et al. A novel upconversion luminescence temperature sensing material: Negative thermal expansion $Y_2Mo_3O_{12}$:Yb^{3+}, Er^{3+} and positive thermal expansion $Y_2Ti_2O_7$:Yb^{3+}, Er^{3+} mixed phosphor. *J. Alloys Compd*. **2021**, *880*, 160156. [CrossRef]
4. Cheng, X.; Zhou, J.; Yue, J.; Wei, Y.; Gao, C.; Xie, X.; Huang, L. Recent Development in Sensitizers for Lanthanide-Doped Upconversion Luminescence. *Chem. Rev.* **2022**, *122*, 15998–16050. [CrossRef]
5. Lin, Y.; Yao, Y.; Zhang, W.; Fang, Q.; Zhang, L.; Zhang, Y.; Xu, Y. Applications of upconversion nanoparticles in cellular optogenetics. *Acta Biomater.* **2021**, *135*, 1–12. [CrossRef]
6. Zhou, J.; Li, J.; Yu, Z.; Li, Z. An upconverted afterglow color conversion strategy for in-situ activated persistent luminescent imaging of medical implants. *Opt. Mater.* **2024**, *152*, 115513. [CrossRef]
7. Zhou, J.; Lei, R.; Wang, H.; Chen, C.; Chen, B.; Pan, E.; Zhao, S.; Xu, S. Er^{3+}/Yb^{3+}-Codoped ZrO_2 Nanocrystals as Ratiometric Luminescence Nanothermometers that Cover Three Biological Windows. *ACS Appl. Nano Mater.* **2020**, *3*, 186–194. [CrossRef]
8. Chen, J.; Zhao, Y.; Mao, Z.; Wang, D.; Bie, L. Investigation of thermal quenching and abnormal thermal quenching in mixed valence Eu co-doped LaAlO3 phosphor. *J. Lumin*. **2017**, *186*, 72–76. [CrossRef]
9. Wang, Y.; Chen, B.; Wang, F. Overcoming thermal quenching in upconversion nanoparticles. *Nanoscale* **2021**, *13*, 3454–3462. [CrossRef]
10. Jahanbazi, F.; Mao, Y. Impact of Negative Thermal Expansion on Thermal Quenching of Luminescence of $Sc_2Mo_3O_{12}$:Eu^{3+}. *Chem. Mater.* **2022**, *34*, 10538–10547. [CrossRef]
11. Zou, H.; Yang, X.; Chen, B.; Du, Y.; Ren, B.; Sun, X.; Qiao, X.; Zhang, Q.; Wang, F. Thermal Enhancement of Upconversion by Negative Lattice Expansion in Orthorhombic Yb2W3O12. *Angew. Chem. Int. Ed*. **2019**, *58*, 17255–17259. [CrossRef]
12. Zou, H.; Chen, B.; Hu, Y.; Zhang, Q.; Wang, X.; Wang, F. Simultaneous Enhancement and Modulation of Upconversion by Thermal Stimulation in $Sc_2Mo_3O_{12}$ Crystals. *J. Phys. Chem. Lett*. **2020**, *11*, 3020–3024. [CrossRef]
13. Liao, J.; Wang, M.; Lin, F.; Han, Z.; Fu, B.; Tu, D.; Chen, X.; Qiu, B.; Wen, H.-R. Thermally boosted upconversion and downshifting luminescence in $Sc_2(MoO_4)_3$:Yb/Er with two-dimensional negative thermal expansion. *Nat. Commun*. **2022**, *13*, 2090. [CrossRef]
14. Lu, Y.; Lin, D.; Li, Y.; Zou, H.; Lu, H.; Zhu, J.; Liu, S.; Li, J.; Zhang, Q. Thermal enhancement of upconversion luminescence in $Sc_2Mo_3O_{12}$: Nd/Yb/Er crystals for optical temperature sensing. *Ceram. Int*. **2023**, *49*, 29370–29374. [CrossRef]

15. Ren, B.; Chen, B.; Zhao, J.; Guo, Y.; Zhang, X.; Chen, X.; Du, Y.; Deng, Z.; Zhu, G.; Wang, F. Synthesis of Core–Shell ScF_3 Nanoparticles for Thermal Enhancement of Upconversion. *Chem. Mater.* **2021**, *33*, 158–163. [CrossRef]
16. Zhou, L.; Wang, W.; Xu, D.; Wang, Z.; Yi, Z.; Wang, M.; Lu, Z. Anti-thermal quenching of Eu3+ luminescence in negative thermal expansion Zr(WO4)2. *Ceram. Int.* **2021**, *47*, 34820–34827. [CrossRef]
17. Yang, Y.; Lin, L.; Lu, P.; Feng, Z.; Li, Z.; Cai, J.; Mei, Z.; Huang, Y.; Guo, W.; Wang, Z.; et al. A linear calibrated high-temperature sensor based on up-conversion fluorescence of $Y_2Mo_3O_{12}$:Er^{3+},Yb^{3+} enhanced by negative thermal expansion. *J. Lumin.* **2021**, *240*, 118410. [CrossRef]
18. Cao, C.; Xie, A.; Zhou, T.; Zhong, H.; Lu, X.; Xie, A.; Noh, H.M.; Jeong, J.H. Eu^{3+} doped lutetium molybdenum oxides: Synthesis, optical properties, thermal behavior, and LED packaging. *J. Lumin.* **2020**, *217*, 116759. [CrossRef]
19. Cheng, Y.; Wang, Y.; Li, D.; Bao, J.; Deng, D.; Guo, H.; Lei, L. Thermal enhancement of upconversion in lanthanide-doped $Gd_2Ti_2O_7$ crystals via fast evaporation in a sol-gel procedure†. *Chem. Commun.* **2022**, *58*, 2327–2330. [CrossRef]
20. Liu, W.; Xu, S.; Lei, L. Enhancing upconversion of $Sc_2Mo_3O_{12}$:Yb/Ln (Ln = Er, Ho) phosphors by doping Ca^{2+} ions. *Opt. Mater.* **2023**, *143*, 114166. [CrossRef]
21. Wei, Y.; Pan, Y.; Zhou, E.; Yuan, Z.; Song, H.; Wang, Y.; Zhou, J.; Rui, J.; Xu, M.; Ning, L.; et al. Frenkel Defect-modulated Anti-thermal Quenching Luminescence in Lanthanide-doped $Sc_2(WO_4)_3$. *Angew. Chem.* **2023**, *135*, e202303482. [CrossRef]
22. Liu, H.; Shao, Z.; Zhu, J.; Zhang, Z. Preparation and property of $(NaZn)^{3+}$-substituted $Sc_2Mo_3O_{12}$ ceramics with negative thermal expansion. *Appl. Phys. Lett.* **2024**, *125*, 181902. [CrossRef]
23. Zhang, Z.; Tian, H.; Zhang, C.; Zhou, Y.; Wang, W.; Meng, X.; Liu, H. Flower-like $Sc_2Mo_3O_{12}$ nanosheet clusters: Synthesis, thermal expansion and photocatalytic properties. *Ceram. Int.* **2022**, *48*, 30135–30143. [CrossRef]
24. Chen, H.; Yu, H.; Cui, S.; Liu, C. Effect of PVP on gas-sensing properties of ZnO micro/nanostructure materials in SDS-PVP composite. *Int. J. Appl. Ceram. Technol.* **2020**, *17*, 1460–1466. [CrossRef]
25. Koczkur, K.M.; Mourdikoudis, S.; Polavarapu, L.; Skrabalak, S.E. Polyvinylpyrrolidone (PVP) in nanoparticle synthesis. *Dalton Trans.* **2015**, *44*, 17883–17905. [CrossRef]
26. Kaniyarakkal, S.; Rajasekharaudayar, K.C.; Dagupati, R.; Li, Y.; Drewniak, S.; Chen, Z.; Nair, V.S.; Edappadikkunnummal, S. Down-/Up-conversion luminescence behaviors and energy transfer analysis in Tm3+ and Tm3+/Yb3+ co-doped tellurite glasses. *Inorg. Chem. Commun.* **2023**, *158*, 111395. [CrossRef]
27. Kshetri, Y.K.; Chaudhary, B.; Dhakal, D.R.; Murali, G.; Pachhai, S.; Lee, S.W.; Kim, H.-S.; Kim, T.-H. Anomalous upconversion behavior and high-temperature spectral properties of Yb/Ho-SiAlON ceramics. *Ceram. Int.* **2023**, *49*, 4807–4815. [CrossRef]
28. Chen, Q.; Xie, X.; Huang, B.; Liang, L.; Han, S.; Yi, Z.; Wang, Y.; Li, Y.; Fan, D.; Huang, L.; et al. Confining Excitation Energy in Er^{3+}-Sensitized Upconversion Nanocrystals through Tm^{3+}-Mediated Transient Energy Trapping. *Angew. Chem. Int. Ed.* **2017**, *56*, 7605–7609. [CrossRef]
29. Wade, S.A.; Collins, S.F.; Baxter, G.W. Fluorescence intensity ratio technique for optical fiber point temperature sensing. *J. Appl. Phys.* **2003**, *94*, 4743–4756. [CrossRef]
30. Cheng, Z.; Lu, J.; Li, Z.; Meng, M.; Qiao, X.; Liu, Y.; Ou, J. Promising lanthanide- $NaYbF_4$:Er^{3+}@$NaYbF_4$:Tm^{3+} micro-phosphors for highly efficient upconversion luminescence and temperature sensing. *Opt. Mater.* **2024**, *154*, 115675. [CrossRef]
31. Pattnaik, S.; Rai, V.K. Insight into the spectroscopic and thermometric properties of titanate phosphors via a novel co-excited laser system. *Mater. Sci. Eng. B* **2021**, *272*, 115318. [CrossRef]
32. Jiang, T.; Wang, X.; Ye, R.; Hua, Y.; Jin, X.; Guo, W.; Liu, G.; Long, Z.; Zhang, B.; Bai, G.; et al. Effects of optically inert ions on up-conversion luminescence and temperature-sensing properties of Y_2O_2S: Er^{3+}/Yb^{3+}/Tm^{3+} phosphors. *J. Alloys Compd.* **2024**, *1000*, 175135. [CrossRef]
33. Wang, R.; Shen, Y.; Zhou, H.; Wang, J.; Zhu, K.; Ye, L.; Yu, X.; Zhang, J.; Wang, L.-G. Up-conversion luminescence and thermal sensing properties of $LuYO_3$: Er^{3+}/Yb^{3+} phosphor. *J. Lumin.* **2024**, *275*, 120799. [CrossRef]
34. Li, J.; Chen, H.; Wang, X.; Li, P.; Lv, M.; Hao, H.; Meng, L. An optical fiber temperature sensor based on fluorescence intensity ratio in Er^{3+}/Yb^{3+} co-doped Gd_2O_3 phosphors. *Ceram. Int.* **2023**, *49*, 28913–28919. [CrossRef]
35. Shuai, P.; Guo, Q.; Liao, L.; Su, K.; Ding, J.; An, N.; Mei, L.; Woźny, P.; Runowski, M. Preparation and sensing performance study in ultra-wide temperature range of K_3LuF_6:Er^{3+},Yb^{3+} up-converting luminescent materials with cryolite structure. *Ceram. Int.* **2024**, *50*, 30879–30886. [CrossRef]

Disclaimer/Publisher's Note: The statements, opinions and data contained in all publications are solely those of the individual author(s) and contributor(s) and not of MDPI and/or the editor(s). MDPI and/or the editor(s) disclaim responsibility for any injury to people or property resulting from any ideas, methods, instructions or products referred to in the content.